Macromolecules

ARTICLE

pubs.acs.org/Macromolecules

Controlling Non-Covalent Interactions to Modulate the Dispersion of Fullerenes in Polymer Nanocomposites

Say-Lee Teh,[†] Dias Linton,[†] Bobby Sumpter,[§,∥] and Mark D. Dadmun*[,†,‡]

[†]Chemistry Department, University of Tennessee, Knoxville, Tennessee 37996, United States

[‡]Chemical Sciences Division, Oak Ridge National Laboratory, Oak Ridge, Tennessee 37830, United States

[§]Computer Science and Mathematics Divisions, Oak Ridge National Laboratory, Oak Ridge, Tennessee 37830, United States

[∥]Center for Nanophase Materials Sciences, Oak Ridge National Laboratory, Oak Ridge, Tennessee 37830, United States

ABSTRACT: Polymer nanocomposites (PNCs) are materials based on a class of filled plastics that contain relatively small amounts of nanoparticles, which can impart improved structural, mechanical, and thermal properties relative to the neat polymer. However, the homogeneous dispersion of the nanoparticles into a polymer matrix is critical and an impeding factor for the controlled enhancement of PNC properties. In this work, we provide new insight into the importance of polymer chain connectivity and nanoparticle shape and curvature on the formation of noncovalent electron donor−acceptor (EDA) interactions between polymers and nanoparticles. This is accomplished by experimentally monitoring the dispersion of nanoparticles in copolymers containing varying amounts of functional moieties that can form noncovalent interactions with carbon nanoparticles with corroboration through density functional calculations. The results show that the presence of a minority of interacting functional groups within a polymer chain leads to an optimum interaction between the polymer and fullerene. Density functional theory calculations that identify the binding energy and geometry of the interaction between the functional monomers and fullerenes correspond very well with the experimental results. Moreover, comparison of these results to similar studies with single-walled carbon nanotubes (SWNT) indicate a distinct difference in the ability of EDA interactions to improve the dispersion of fullerenes relative to their impact on SWNT. Thus, the polymer chain connectivity, the polymer chain conformation, and size and shape of the nanoparticle modulate the formation of intermolecular interactions and directly impact the dispersion of the resultant nanocomposite.

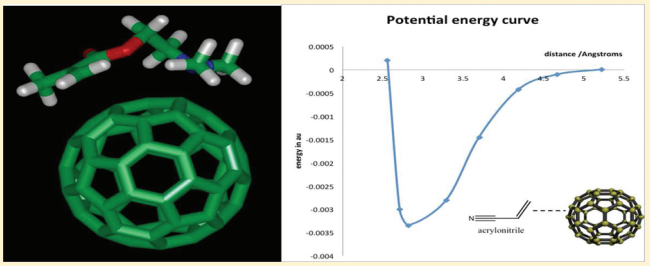

INTRODUCTION

Polymer nanocomposites (PNCs) open a new horizon for polymeric-based materials with properties that are a synergistic combination of both the polymer, which are lightweight, strong, environmentally inert, and cost efficient,[1,2,5] and nanoparticle substituents, which can enhance the mechanical, electrical, and thermal properties of the resulting material.[10] Nanocomposites offer the possibility for significant property improvement with a minimal addition of filler, where property increases on the order of ∼10% can readily be achieved.[3] For example, PNCs can exhibit significant improvement in mechanical reinforcement, even with a filler content as low as 1 wt %.[2,11] The ability of PNCs to confer significant property improvements with very low loading has resulted in their replacement of conventional microcomposites in commercial applications, such as the automobile industry.

It is well-known that the performance of a polymer nanocomposite depends significantly on nanoparticle dispersion and the interfacial adhesion between the nanoparticle and the polymer matrix. Numerous studies have shown that improved interactions between a polymer matrix and the reinforcing phase lead to improved mechanical properties.[4−7] For instance, Zhu et al. demonstrated that the presence of a strong hydrogen bonding interaction between a polyurethane/epoxy resin interpenetrating network and a montmorillonite nanoparticle creates a resultant polymer nanocomposite that exhibits improved miscibility and efficient chain packing.[8] In addition, the shape of the nanoparticles can dramatically influence the extent of interaction between the polymer matrix and nanoparticle and impact the influence of nanoparticle presence on the polymer chain structure and dynamics. If the nanoparticles are well dispersed in the polymer matrix, the added nanoparticles, which have a very high surface to volume ratio, can significantly alter the dynamics of the surrounding polymer matrix as a result of this extraordinary amount of interfacial area. For instance, Mackay et al. report that the dispersion of soft nanoparticles can swell the polymer and reduce the viscosity of the polymer below that of a traditional composite,[9] where the swelling of the polymer results in an increase of 10−20% in the radius of gyration of *d*-polystyrene.

Received: April 5, 2011
Revised: August 15, 2011
Published: September 13, 2011

ACS Publications © 2011 American Chemical Society

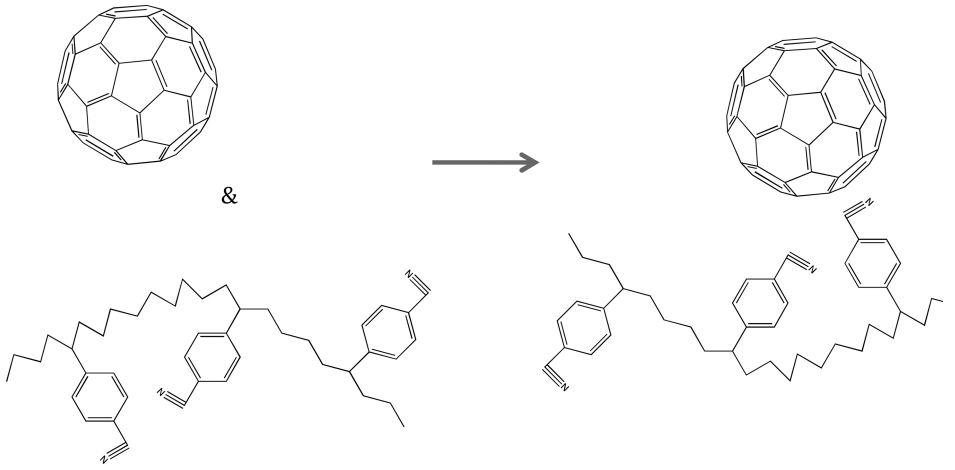

Figure 1. Illustration of the formation of an electron donor−acceptor (EDA) interaction.

As the improvement of targeted properties depends on the dispersion of nanoparticles in a polymer matrix, methods to improve the homogeneity of polymer nanocomposites have become an intense area of study. One common method to improve the dispersion of a polymer nanocomposite is to incorporate intermolecular interactions between the polymer matrices and the nanoparticles, either covalent or noncovalent. Electron donor−acceptor (EDA) interactions are particularly interesting for polymer-carbon nanoparticle nanocomposites, as the aromatic structure of single-walled carbon nanotubes (SWNTs), graphene, or fullerenes provides an environment that can readily form a noncovalent electron transfer interaction from one electron rich component to the other electron deficient component.[10,11] Moreover, these nanoparticles are amphoteric and can behave as electron donors or electron acceptors depending on their environment. For instance, fullerenes or single-walled carbon nanotubes can form a complex with polymer-bound cyano groups to create a weak attractive noncovalent interaction between the donor and the acceptor (Figure 1). The incorporation of this attractive molecular interaction between components is expected to improve the dispersion of nanoparticles due to the enthalpic attraction between the nanoparticles and the surrounding polymer matrix.

The effects of electron donor−acceptor interactions between a polymer-bound functional group and single walled carbon nanotubes have been previously examined in our group.[12] Experimental and computational results detail the importance of chain connectivity and steric effects in determining the extent of noncovalent electron donor−acceptor interactions that can form between polymer-bound functional groups and the SWNTs. In the current article, we describe an extension of this work to examine the ability of similar functional groups to improve the dispersion of fullerenes in polymer matrices, documenting the importance of nanoparticle size and shape on the formation of EDA noncovalent interactions and its impact on dispersion.

In a similar study, Rasheed and co-workers demonstrated the importance of steric effects and the accessibility of polymer-bound functional groups to form hydrogen bond interactions between a polymer and single-walled nanotubes.[13−16] These experiments indicated that inclusion of 20% vinyl phenol on a polymer chain optimizes the formation of intermolecular hydrogen bonds between the polymer and the oxidized CNT. Interestingly, Linton et al. reported similar results for the incorporation of noncovalent electron donor−acceptor interaction between polymer-bound functional groups and SWNTs.[12] The results were interpreted to indicate that the accessibility of a polymer-bound functional group to approach and align correctly with the nanoparticle surface dramatically impacts the success of intermolecular noncovalent interaction formation. If one polymer-bound functional group forms an intermolecular interaction, this dynamic confinement can limit the ability of neighboring (polymer-bound) functional groups to also form an intermolecular interaction. Separation of functional groups along the polymer chain confers sufficient dynamic independence to improve the probability of interaction formation and thus results in an optimum functional group composition in these interacting nanocomposites.

This understanding of connectivity effects in the formation of noncovalent interactions in polymer nanocomposites leads to the question of the importance of the size and shape of the nanoparticle on the formation of noncovalent interactions. Nanoparticles that are added to polymers can take a variety of shapes, including spheres, cylinders, and sheets. As previous results clearly demonstrated that chain connectivity could limit the ability of a polymer-bound functional group to readily form desirable intermolecular interactions, it would also appear that the specific size, shape, and curvature of the nanoparticle could also influence the formation of these interactions. Therefore, to more thoroughly understand the ability of EDA interactions to optimize the dispersion of a broad range of nanoparticles in a polymer matrix, we carried out experiments designed to determine the effect of nanoparticle size, shape, and curvature on the formation of noncovalent interactions and its influence on the homogeneity of the resultant nanocomposite. In this study, the amount of electron donating (DMAEMA) or electron withdrawing (AN and CNSt) moieties in three sets of copolymers were varied between ∼10 to 50 mol %. The impact of these structural modifications of the polymer chain on the dispersion and polymer dynamics are examined experimentally. These results are combined with quantum density functional theory calculations to provide insight into the ability of using noncovalent interactions to control the dispersion in polymer-fullerene nanocomposites.

■ EXPERIMENTAL SECTION

In this study, we examine the ability of specific functional groups to improve the dispersion of fullerenes in polymer matrices and demonstrate

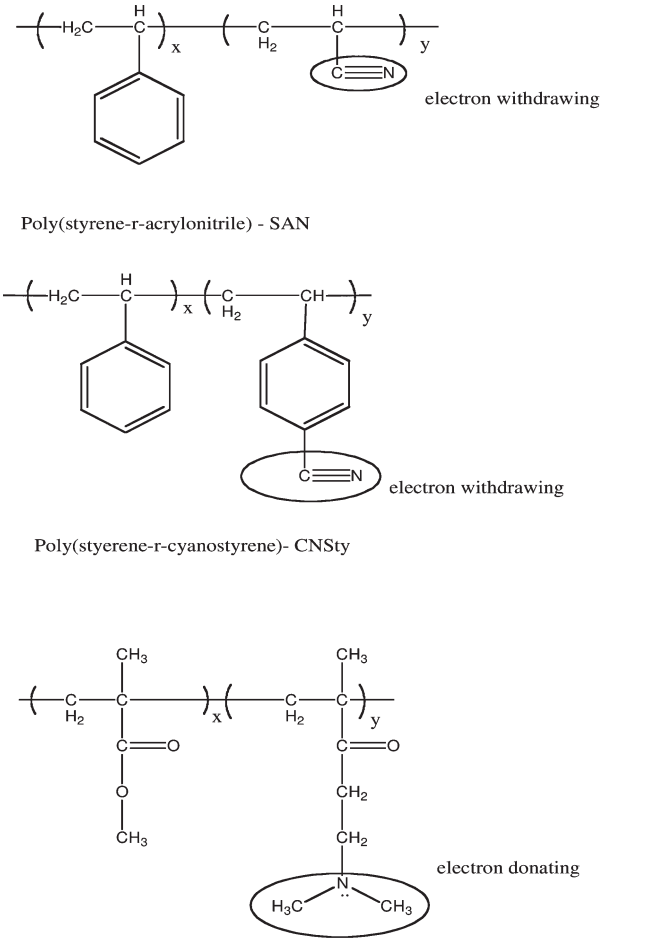

Figure 2. Structures of the copolymers used in this study.

the importance of nanoparticle size and shape on the formation of EDA noncovalent interactions and its impact on dispersion. To realize this, the electron accepting nitrile functional group (−CN) is introduced in poly(cyanostyrene-*ran*-styrene) (PCNSty/Sty) and poly(styrene-*ran*-acrylonitrile) (SAN) copolymers, and the electron donating amino group is introduced in poly(dimethyl amino ethyl methacrylate-*ran*-methyl methacrylate) (PDMAEMA-MMA) copolymers. The impact of the presence of the varying amount of these functional moieties on the structure and dynamics of polymer nanocomposites is subsequently examined. Figure 2 shows the structure of the copolymers used in this study, and Table 1 lists their compositions.

Materials. Styrene, dichloromethane, and 4-cyanostyrene monomers were purchased from Acros Organics, and 2,2′-azobisisobutyronitrile (AIBN), 1,1,2,2-tetrachloroethane, and *N*,*N*-dimethyl acetamide were purchased from Sigma Alrich. *N*-hexane and methanol were purchased from Fisher Scientific. Poly-2-(dimethylamino ethyl methacrylate) (PDMAEMA), polystyrene (PS), and polyacrylonitrile were obtained from Scientific Polymer Products, Inc. Styrene-*ran*-acylonitrile copolymers (SAN) with 29.4, 36.8, 45.05, 48.8, and 56.2 mol % AN were obtained from an industrial source. The C_{60} fullerenes were purchased from Bucky USA and used as received (99.5% purity).

Synthesis of Random Copolymers. Methyl methacrylate-*ran*-DMAEMA copolymers were synthesized via atom transfer radical polymerization using CuCl complexed by bipyridine (bpy) as the catalyst and *p*-toluene sulfonyl chloride (*p*-TsCl) as the initiator. The monomers, CuCl, bpy, *p*-xylene (v/v % of solvent to monomer ∼80%), and

Table 1. Composition of Each Copolymer Used in This Study

SAN		CNSty/Sty		P (MMA-DMAEMA)	
styrene mol %	AN mol %	CNSty mol %	Sty mol %	DMAEMA mol %	MMA mol %
70.5	29.5	16.0	84.0	12.2	87.8
63.2	36.8	22.3	77.7	26.3	73.7
55.0	45.0	28.5	71.5	30.4	69.6
51.2	48.8	43.1	56.9	49.2	50.8
43.77	56.23				

p-TsCl were introduced, in this order, into a 250 mL 2-necked round-bottom flask that was equipped with a reflux condenser and a stir bar. The molar ratio of *p*-TsCl initiator, CuCl, and bpy ligand used was 1:6:12. The mixture was immediately degassed by three freeze−pump−thaw cycles to remove trace impurities. The flask was heated in an oil bath at 90 °C for 18 h under nitrogen flow with continuous stirring. The resulting copolymers and homopolymer were diluted and passed through an alumina column twice to eliminate copper residues before they were precipitated in a 10-fold excess of cold *n*-hexane. These samples were then dried under vacuum at 70 °C for 2 days.

Free radical polymerization was also used to copolymerize styrene and cyanostyrene. In this reaction, a 1:1 volume ratio of solvent *N*,*N*-dimethylacetamide (DMAc) to monomer is used. A typical reaction procedure is illustrated for the polymerization of the copolymer containing 20 mol % cyanostyrene. In this reaction, styrene (19.3 g, 0.19 mol), 4-cyanostyrene (1.8082 g, 0.014 mol), AIBN (0.07652 g, 0.47 mmol), and DMAc (21.1 mL) were combined in a two neck round-bottom flask under nitrogen flow, equipped with a reflux condenser and stir bar. The mixture was subjected to three freeze−pump−thaw cycles to ensure the removal of oxygen. The temperature of the flask was raised by immersion in a hot oil bath at 65 °C for approximately 20 h with continuous stirring and nitrogen flow. The polymer was precipitated in a 10-fold excess of cold methanol with rapid stirring. The polymer was then dried in a vacuum oven overnight to remove any remaining solvent.

Preparation of Polymer Nanocomposites. The SAN/C_{60} nanocomposite samples were prepared from toluene solutions, while the MMA-*ran*-DMAEMA/C_{60} and styrene-*ran*-cyanostyrene/C_{60} composites were prepared from 1,1,2,2-tetrachloroethane (TCE) solutions. In the preparation of these nanocomposites, C_{60} was added to the solvent (2 mg/mL concentration), and the mixture was sonicated until a purple solution was produced. The copolymer (∼0.5 g) was then added to the appropriate solvent (concentration: 0.1 g/mL), and the mixture was vortexed, resulting in the formation of a transparent solution. The C_{60} solution was then added dropwise to the copolymer solution to achieve the targeted polymer/C_{60} composition ranging from 0.5 to 5.0 wt %. The combined solutions were homogenized by further sonication for approximately one hour. The resulting solutions were precipitated in a 5-fold excess of cold methanol with continuous stirring, and the resulting mixture was left in the refrigerator at 4 °C for 12 h. The product was then collected by vacuum filtration, and the composite was dried under vacuum at room temperature overnight.

The dried composite was compressed onto a thin aluminum mold (1 cm × 2 cm × 0.05 cm) with Kapton sheets sandwiched between two plates. These samples were compression molded above the glass transition temperature, T_g, of the polymer at a pressure of ∼10,000 lbs for a duration of about 5 min.

Polymer Characterization. *Gel Permeation Chromatography (GPC).* Gel permeation chromatography was used to determine the molecular weight characteristics of the polymers used in this study. Measurements were performed on a Polymer Lab GPC-20 instrument

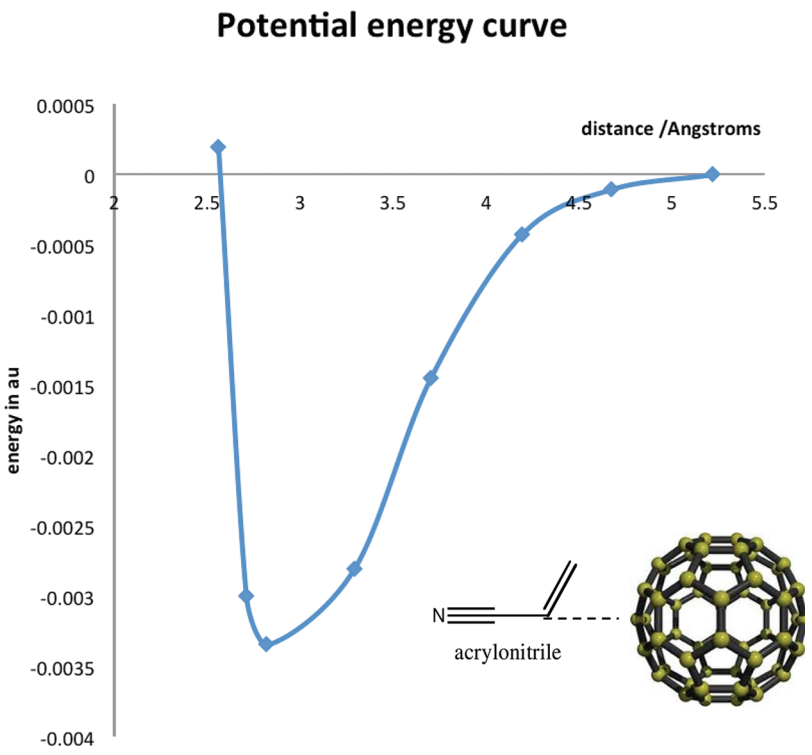

Figure 3. Potential energy curve of AN-C_{60} with the C−C bond of AN aligned to the center of the hexagon on C_{60}.

with 300 mm × 7.5 mm Polymer Laboratories 5 μm Mixed C columns, a 50 mm × 7.5 mm Polymer Laboratories 5 μm guard column, and a Knauer K-2301 differential refractometer as a detector. Samples were prepared at 1 mg/mL concentration in HPLC grade THF, stabilized with 100 ppm butylated hydroxyl toluene (BHT) as the mobile phase. In addition, the samples were filtered through a 0.45 μm syringe filter prior to injection.

Nuclear Magnetic Resonance (NMR). Nuclear Magnetic Resonance (NMR) was used to determine the composition of the St-*ran*-CNSt. Samples were prepared as 7 mg/mL in deuterated chloroform, and the chemical shift scale was referenced to the tetramethylsilane peak at 0 ppm. The measurements were carried out on Varian 250 MHz and Varian 400 MHz NMR spectrometers.

The ^{1}H NMR peak assignment for poly(styrene-*ran*-cyanostyrene) are 7.08−7.43 ppm multiplet 9H aromatic protons; 2.76−2.94 ppm singlet 2H−CH; 1.58 ppm doublet 1H−CH_2. The ^{13}C NMR spectrum confirmed the incorporation of the nitrile group from cyanostyrene in the copolymer with a characteristic peak at the chemical shift δ = 119.1 ppm.

Elemental Analysis. Elemental analysis was completed by Atlantic Microlab Inc. (Norcross GA) to determine the composition of the St-*ran*-CNSt and SAN copolymers. This analysis provided the weight percent of C, H, and N present in the sample, with an error of ±0.3%. The mol percent of each functional group in the synthesized copolymers was calculated from these reported values.

Characterization of Polymer Nanocomposites. *X-ray Diffraction (XRD).* XRD patterns of the polymer nanocomposites were obtained using a Rigaku, Inc. XRD instrument at room temperature, using monochromatic Cu Kα radiation operating at 45 kV and 0.66 mA. Data were collected for 2θ ranging from 5 to 35 degrees. The appearance of C_{60} crystalline peaks was taken as a measure of the miscibility limit of the C_{60} in the polymer matrix as described below.

Differential Scanning Calorimetry (DSC). Differential scanning calorimetry measurements were carried out on Mettler Toledo DSC 821 and TA Instruments Q1000 DSC with nitrogen as the purging gas. The calibration of the DSCs was performed using indium as a standard (mp 156.6 °C and heat of fusion = 28.45 J/g). Samples, weighing 10−15 mg, were heated from 60 to 160 °C at a rate of 10 °C/min, with a nitrogen flow rate of 200 mL/min.

The samples were heated to ∼10−15 K above the glass transition, T_g, where the samples were annealed at this temperature for a short period of time (3−5 min) to erase the thermal history of the system. This was followed by a rapid cooling to a temperature of at least 40 K below the glass transition and immediate reheating at a constant rate. The thermal properties of the polymers and polymer nanocomposites were determined by completing duplicate measurements. The midpoint of the heat capacity change of the second consecutively identical scan was recorded as the glass transition temperature, T_g.

RESULTS

Density Functional Theory (DFT). All electron density functional theory (DFT) is used to provide information on the interaction strength between the functional monomers and a C_{60} fullerene (specific details on the optimization procedure used to determine the structures and binding energy can be found in ref 12). The structures of the all monomer-C_{60} complexes were fully optimized in Cartesian coordinates, using both the local density approximation (LDA) and generalized gradient approximation (GGA).[17] The results discussed and presented in the figures and table correspond to those obtained from LDA unless otherwise specified. It is now well-known that ab initio DFT methods often can exhibit significant errors for nonbonded interactions unless very large basis sets are used in conjunction with highly correlated methods such as coupled-cluster with perturbative triple excitations, CCSD(T).[18] While most popular density functional approximations fail to describe London dispersion interactions, a large number of studies have sought to improve theoretical methods for nonbonded interactions. The simplest method is

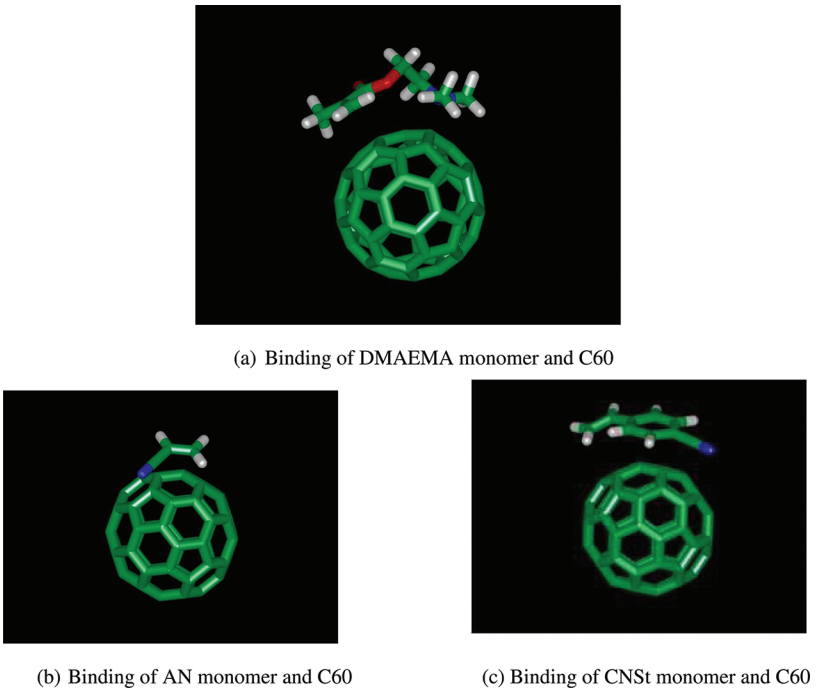

(a) Binding of DMAEMA monomer and C60

(b) Binding of AN monomer and C60

(c) Binding of CNSt monomer and C60

Figure 4. Optimized geometries of the C_{60} complexes with different monomers that contain electron donating or accepting moieties interacting with C_{60}.

based on adding a damped, empirical dispersion term, yielding a method designated as DFT-D.[18] This approach is simple and cost-effective and has demonstrated excellent results for nonbonded interactions in a variety of geometries. In the present study, we have used DFT/GGA and DFT-D calculations to verify that the trends observed are not significantly modified due to these corrections in DFT/LDA.

These results can be compared to similar calculations of the interaction between the same monomers and SWNTs to provide insight into the role of nanoparticle size and curvature on the formation of the EDA interaction. One such calculation is illustrated in Figure 3, which shows the potential energy curve of the C_{60}-acrylonitrile interaction as a function of distance between the C_{60} face and the monomer using the DFT with the Gaussian basis set, 3-21G. The points shown in Figure 3 are corrected for basis set superposition error (BSSE) and deformation energy correction.[18,19] BSSE is used to account for a finite basis set (3-21G) and the deformation energy because of small structural changes that occur for the monomer and C_{60}. This is a standard protocol for computing interaction energies using quantum chemistry methods for finite sized systems and basis sets. In Figure 3, the total interaction energy between the acrylonitrile (AN) monomer and C_{60} is plotted as a function of the distance between the AN monomer (center of mass) and C_{60} (center of a hexagon on the face).

Figure 4a shows the optimized geometry for the DMAEMA-C_{60} interaction, where the alignment of the N atom on the DMAEMA monomer with the C atom on C_{60} produces a strong interaction. Figure 4 provides some insight into the proximity that the free monomers can attain to the C_{60} to form an optimum noncovalent interaction. Interestingly, Figure 4c shows that the alignment of the phenyl ring on CNSt is neither face-to-face tangential nor parallel with a hexagon on C_{60}. This odd angle for alignment results in a larger distance between the C on CNSt and C on C_{60} than other monomers, as well as a larger distance between the CN group to C on C_{60}. Due to these large distances, the binding energy of CNSt with C_{60} is significantly lower than that of the interaction between CNSt with SWNT.[12] These results exemplify the importance of the curvature and size of the nanoparticle in the formation of noncovalent interactions, where conformity of the functional group to the surface of the nanoparticle appears to be an important process.

To summarize the results of this analysis, the distances between the monomers and C_{60} in their optimized geometry are shown in Table 2, along with the binding energy between the monomer and C_{60} as well as between the monomers and a (8,0) SWNT. It is important to note that such intra- and intermolecular distances are typically found to be accurate to within 0.01 Å for systems that have been compared to X-ray data.

Table 2 quantifies the level of interaction between fullerene and each monomer, as the smaller the distance between the functional group and fullerene, the stronger the potential intermolecular interactions in the polymer nanocomposites. It is worth noting that the distance between the carbon in styrene and the carbon in C_{60} is relatively close, which may be associated with a $\pi-\pi$ interaction. Similarly, the distance between the carbon in C_{60} and the carbon in cyanostyrene, which consists of an aromatic phenyl ring and a nitrile group, is only slightly larger.

These results demonstrate the importance of the nanoparticle shape on the formation of the EDA interaction. The highly curved fullerene cannot fully accommodate the $\pi-\pi$ and EDA interaction of the cyanostyrene due to its size, resulting in a smaller binding energy of 2.4 kcal/mol. This can be contrasted to the interaction of CNSt with SWNT, as shown in Figure 5, where both the EDA and $\pi-\pi$ interactions can be realized by positioning the monomer along the length of the tube, resulting in a binding energy of 10 kcal/mol. Therefore, the specific curvature of the nanoparticles demands that the functional group attain

Table 2. Closest Distance between Monomer and C_{60} in the Optimized Geometry, Computed Binding Energy for the Same Monomer and a (8,0) SWNT, and the Binding Energy for C_{60}

monomer	distance C(monomer)−C (C_{60}) (Å)	distance C_{60}−functional group (Å)	(8,0) SWNT (kcal/mol)	C_{60} (kcal/mol)
acrylonitrile	3.02	(C → N) = 3.27	4.5	2.1
cyanostyrene	2.67	(C → N) = 3.79	10.0	2.4
DMAEMA	2.91	(C → N) = 1.87	0.3	4.7
methyl methacrylate	3.13	(C═O → C) = 2.64	0.6	1.4
styrene	2.63	N/A	1.9	3.2

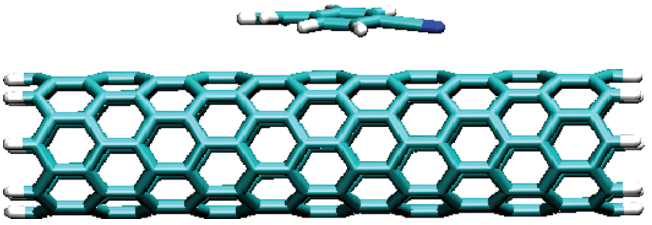

Figure 5. Optimized geometry between (8,0) SWNT and CNSt, showing the aromatic phenyl ring facing the SWNT π network.

different optimum geometries, resulting in differing binding energies. The aromatic structure of CNSt readily binds with SWNT in a flat position with its sp^2 resonance facing the π network structure between the monomer and SWNT. However, the smaller binding energy of CNSt with C_{60} is the result of the limited alignment afforded by the curvature of the C_{60} sphere.

These computational results also show that the interaction between C_{60} and the amine group in the DMAEMA monomer has the highest binding energy, 4.73 kcal/mol, twice that of CNSt. The optimized geometry of the DMEAMA monomer and C_{60} shows that the N atom is directly above a carbon on the C_{60} and creates a relatively strong interaction. This is clearly a result of the flexibility of the DMAEMA monomer allowing the DMAEMA to conform to the shape of the highly curved C_{60} considerably more than the CNSt.

Interestingly, styrene exhibits a relatively high binding energy with C_{60} among the monomers studied. The binding energy of 3.21 kcal/mol between fullerene and styrene is stronger than that between C_{60} and AN or between C_{60} and CNSt. Styrene is able to interact with C_{60} via $\pi-\pi$ interactions between the curved π surface of the C_{60} cage and the flat π surface of the phenyl ring of polystyrene. In addition, the distance between C_{60} and PS is also relatively small, ~2.63 Å, indicating the strong interaction between the nanoparticle and the monomer. This proximity is also true for the CNSt monomer. As a result, CNSt is the third strongest binding monomer with a binding energy of 2.4 kcal/mol. These results suggest that $\pi-\pi$ stacking interactions that occur in the polymer nanocomposites with the phenyl ring on the polymer chains play a significant role in the dispersion of C_{60} in these particular polymers.

Differential Scanning Calorimetry (DSC). Differential scanning calorimetry is used to measure the thermal properties of the fabricated nanocomposites and is used in this study to monitor the change in the glass transition, T_g, of the polymer with the

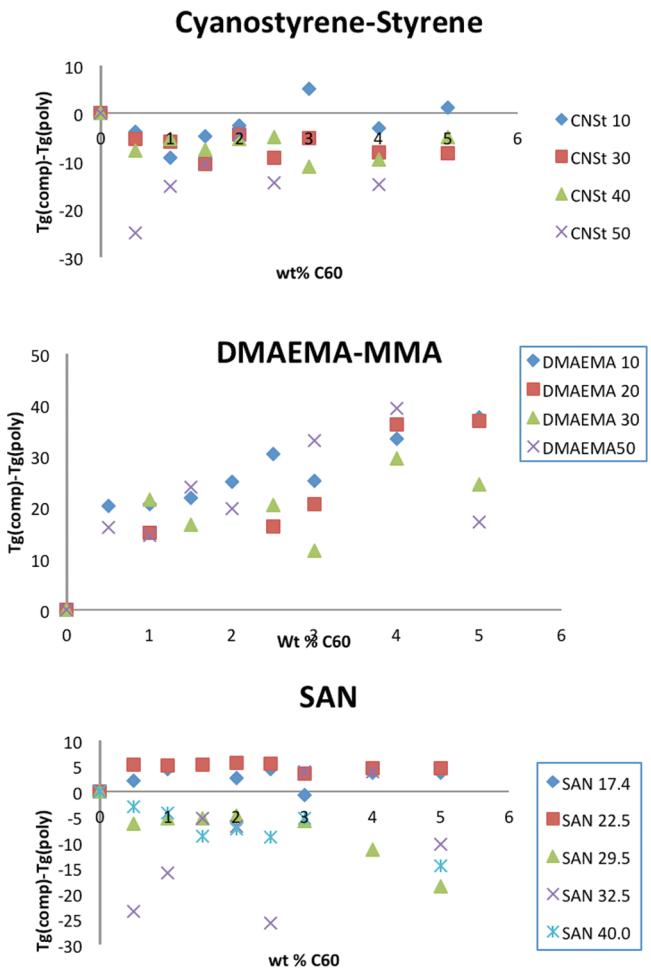

Figure 6. Graph of the change in T_g, [T_g(composite) − T_g(polymer)], with the addition of C_{60} to (top) CNSt copolymers, (middle) DMAEMA copolymers, and (bottom) SAN copolymers.

addition of a nanoparticle. This information is interpreted to indicate the presence or absence of intermolecular interactions between the polymer and nanoparticle.

An enhancement in the T_g of a polymer upon the addition of a nanoparticle is interpreted as the result of the presence of a strong interaction between the nanoparticles and the polymer, as this interaction reduces molecular mobility and flexibility of the polymer chain in the vicinity of the nanoparticle. However, previous studies of the change in T_g with the addition of a nanoparticle demonstrate that T_g may increase or decrease with the addition of nanoparticles.[20,22] For instance, Starr et al. reported that a nanocomposite with an attractive interaction between components exhibits an increase in T_g by approximately 6% for a particle loading of 8 wt %, while nanocomposites with no attractive interactions between components show a decrease in T_g by a similar amount.[21] Similarly, Lu and Weiss demonstrated that an increase in T_g represents strong interactions, while a decrease in T_g is the result of weak interactions.[22] The authors interpreted their results to indicate that particles with a strong polymer−particle interaction give rise to an increase in T_g, reflecting its immobilization. In addition, Wong et al. reported that the presence of C_{60} can alter the high frequency local dynamics of a polymer with an increase in T_g and slow chain dynamics.[23] Clearly, the presence and strength of the

polymer−particle interaction modifies the polymer dynamics, exhibiting behavior that differs from that of the neat polymer.

The DSC results for the C_{60} nanocomposites studied here, which show the T_g of the polymer as a function of C_{60} present in the nanocomposite, are shown in Figure 6, where the uncertainty is on the order of the symbol size. These results show that the incorporation of C_{60} into AN, CNSt, and DMA impacts the dynamics of the polymer matrix differently. Generally, an increase of T_g in the DMAEMA-C_{60} nanocomposites is observed for all samples, while the T_g of the CNSt-C_{60} nanocomposites generally decreases, and the T_g of the SAN-C_{60} nanocomposites exhibits a copolymer composition dependent increase or decrease in T_g.

Guided by the computational results, these observations can be explained by correlating the observed polymer chain dynamics to the polymer nanocomposite dispersion and interaction between fullerene and the functional groups in each copolymer. The interpretation of these results, therefore, provides remarkable insight into the role of nanoparticle size and shape, as well as polymer chain flexibility, in the formation of noncovalent interactions in polymer fullerene nanocomposites.

The data reported in Figure 6 is the change of T_g, ΔT_g (ΔT_g = T_g(nanocomposite) − T_g(copolymer)), of the polymer chain upon addition of fullerene, as a function of copolymer composition. Figure 6, middle, shows an increase in T_g with the addition of fullerene for the DMAEMA copolymers, which is interpreted to be the result of strong interactions between the copolymer and C_{60}. Conversely, the CNSt nanocomposites exhibit a consistent decrease in T_g with incorporation of the fullerene. Following previous studies cited above, this negative deviation of T_g is interpreted to indicate the presence of weak interactions between a polymer and nanoparticle, which increases the mobility of the polymer chain in the vicinity of the nanoparticle.

The SAN nanocomposite trend is more complex with an increase in T_g for copolymers with low AN content and a decrease in T_g at higher AN compositions. EDA complexes are created when the electron withdrawing nitrile group of AN on a polymer chain is in close proximity to the carbon cage of C_{60}. These results appear to indicate that for copolymers with low AN content, strong intermolecular interactions exist that limit polymer mobility. After an optimal amount of AN groups has been incorporated into the copolymer matrix, further increasing AN concentration results in a decrease of T_g, indicating a decrease in the extent of interactions between the polymer and fullerene.

The difference in the behavior of the SAN and CNSt polymers can provide an important insight into the role of chain flexibility and steric crowding on the formation of noncovalent interactions in these systems, as both polymers contain phenyl rings, which can participate in $\pi-\pi$ interactions, and nitrile groups that can form EDA complexes with the fullerenes. Yet, given this similarity of structure, their behavior in the T_g studies differs significantly. The CNSt polymer chain contains a bulky phenyl ring on every monomer, which may inhibit the ability of sufficient functional groups to orient and position in proximity to a fullerene molecule to form EDA and/or $\pi-\pi$ interactions. This poor packing, therefore, should result in an increase in free volume and a decrease in the measured T_g. The SAN copolymer, however, contains the smaller, more flexible acrylonitrile groups in the polymer chain, which permits the formation of more $\pi-\pi$ and EDA interactions. However, increasing the AN content decreases T_g, which implies that the loss of the styrene and $\pi-\pi$ interactions dominates the response of the system, not merely the polymer flexibility. This can be further interpreted to indicate that the $\pi-\pi$ interactions are dominant relative to the EDA interaction between the fullerene and the nitrile group, a conclusion that correlates extremely well to the density functional theory results. This interpretation is consistent when comparing both the CNSt and SAN systems, exemplifying the role of $\pi-\pi$ and EDA interactions between fullerenes and copolymers in determining their dispersion.

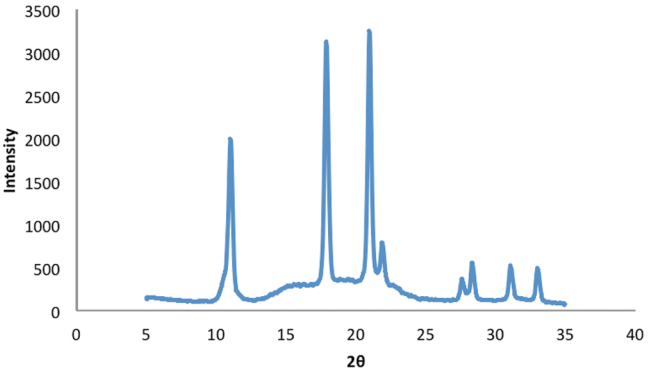

Figure 7. X-ray diffraction spectra of pure C_{60}.

In addition, these results are also consistent with the current understanding of the electron affinity of fullerenes. Fullerenes are widely known to have a very high electron affinity, as they are capable of accepting at least 6 electrons upon reduction (i.e., act as an electron acceptor).[24−26] The detection of C_{60}^{2-}, C_{60}^{3-}, C_{60}^{4-}, C_{60}^{5-}, and C_{60}^{6-} ions electrochemically provides experimental evidence of the triple degeneracy of the lowest unoccupied molecular orbital (LUMO) of fullerene.[26] Similarly, theoretical and experimental results show that the oxidation (i.e., donation of an electron) of C_{60} is more challenging.[26] It is, therefore, not surprising that the MMA/DMAEMA copolymer disperses the fullerenes more readily and forms stronger EDA interactions than the copolymers containing the nitrile group, the SAN and St/CNST copolymers. However, it should be stressed that the polymer matrix electron donicity alone is not solely responsible for the control of fullerene dispersion. If this were true, DMA10 would have a lower T_g than copolymers having a higher amount of DMAEMA functional groups. Since this is not the case, there must be other factors that affect the extent of intermolecular interaction and dispersion, which strongly suggests that that polymer chain connectivity, particle size, shape, and curvature influence the formation of these interactions.

X -Ray Diffraction (XRD). X-ray diffraction experiments are completed to estimate the miscibility limits of C_{60} in the polymer matrices. In the absence of polymers, C_{60} forms a crystalline structure, where the first three peaks in the XRD pattern are at 2θ ~11°, 18°, and 21°, as shown in Figure 7. When the C_{60} is added to the polymer matrix, these peaks will disappear if the fullerene is homogenously dispersed in the polymer matrix but will be present as the C_{60} phase separates[11] since C_{60} is known to readily crystallize due to its closed packed structure.[27] Therefore, the presence or absence of the C_{60} crystalline peaks in the diffraction spectra can be used to delineate the miscibility of the fullerene in the polymer matrix. To realize this, the XRD patterns of the polymer-fullerene nanocomposites with varying C_{60} loadings were obtained and analyzed. The nanocomposite with the lowest C_{60} content that exhibits the C_{60} crystalline peaks is assigned as the miscibility limit of fullerene in the corresponding

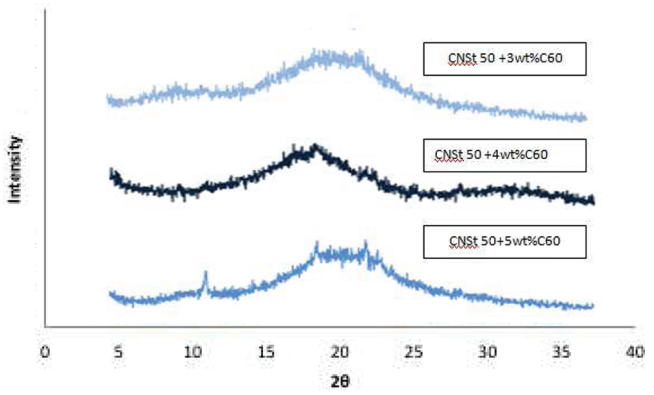

Figure 8. X-ray diffraction patterns of CNSt50 nanocomposites with increasing C_{60} loadings.

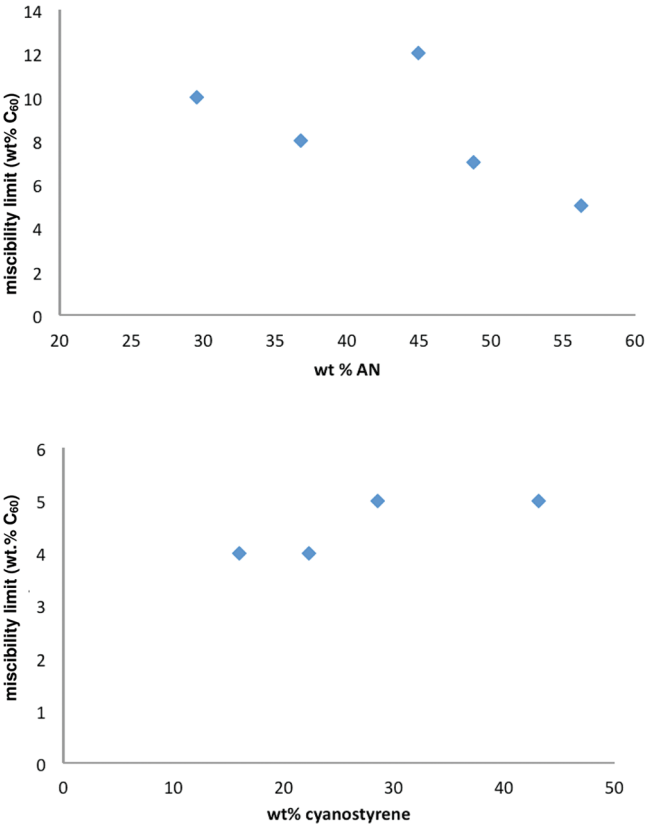

Figure 9. Miscibility limit of C_{60} in (top) SAN and (middle) CNST as a function of copolymer composition.

polymer matrix.[11] In these experiments, diffraction patterns were recorded from $2\theta = 5°$ to 35° at a scanning speed of 1°/min.

Figure 8 shows the X-ray diffraction patterns for a set of the C_{60} nanocomposites with the CNSt50 copolymer. The broad amorphous peak in the XRD spectra of the 3 wt % C_{60} and 4 wt % C_{60} nanocomposites indicates a miscible sample or the absence of C_{60} crystalline material. Meanwhile, sharp crystalline peaks appear in the 5 wt % C_{60} sample, indicating the onset of phase separation of the C_{60} from the polymer matrix. The lower limit of detection of this crystal peak is estimated to be ~3 wt %. This procedure was completed for each copolymer studied, and the resultant C_{60} miscibility limits are shown in Figure 9 for the CNSt and SAN copolymers, where the uncertainty is ±0.5 wt %.

In Figure 9, the 45 mol % AN copolymer shows the highest miscibility limit of the SAN copolymers, at approximately 12 wt % C_{60}. This agrees with previous work in our lab that showed similar behavior of SAN-SWNT nanocomposites, where the 45% AN copolymer exhibited optimal dispersion for this copolymer.[12] For CNSt, there is no clear optimal copolymer composition, but the C_{60} miscibility limit of these nanocomposites is only 5%, significantly lower than that of the SAN copolymers. This agrees, qualitatively, with the DSC results, which indicate that the flexibility of the SAN copolymer chain allows the formation of more intermolecular interactions between a polymer and a small, spherical nanoparticle. This translates into a higher miscibility limit of the SAN samples than that of the CNSt series.

The miscibility limit of the DMAEMA copolymer with 50% DMAEMA was also studied, where the results showed no crystalline C_{60} (by XRD) up to 20 wt % C_{60}. Therefore, the miscibility limit of C_{60} in this copolymer is at least 20 wt %, probably higher. This ability to incorporate a significant amount of fullerene into the polymer matrix is consistent with the DFT and DSC results presented above. The DFT results clearly show that the DMAEMA monomer can approach the C_{60} sphere and align itself properly to realize an interaction with the strongest binding energy of the monomers studied. This enthalpic attraction between the polymer and fullerene manifests itself as an increase in the glass transition temperature of all DMAEMA containing polymer chains upon addition of the fullerene and also appears to significantly increase the miscibility of the polymer and fullerene, though further experiments are underway to more precisely define these limits.

SUMMARY

The results presented in this article demonstrate that the level of dispersion of C_{60} fullerene in a polymer matrix and the properties of the resultant nanocomposite can be effectively modulated by the presence of noncovalent interactions between the polymer and nanoparticle additive. In particular, a comparison of the behavior of cyanostyrene-styrene copolymers and styrene-acrylonitrile copolymers indicates that $\pi-\pi$ stacking interactions with phenyl rings on the polymer chains play a key role in determining the dispersion of the fullerene in the copolymers.

The results also show that the dispersion is optimal when a minority of noncovalent interacting functional groups is present in a SAN matrix. This implies that polymer chain connectivity impacts the formation of noncovalent interactions and is critical to obtain an optimal dispersion of a nanoparticle in a polymer matrix. The specific copolymer composition that optimizes the formation of the EDA interaction is dependent on geometrical constraints, flexibility, and structure of the monomers in the copolymer.

Among the three different copolymers (SAN, CNSt, and DMAEMA), the DMAEMA copolymer exhibits the most homogeneous nanocomposites with C_{60}. There exists a strong correlation between experimental and computational results, where the density functional theory calculated interaction energies and the distance between components in their optimized geometry corroborates the experimental data. The results indicate that DMAEMA forms the strongest intermolecular interaction with C_{60}, followed by styrene, acrylonitrile, and CNSt. This further affirms

the observation that C_{60} forms strong $\pi-\pi$ interactions. It also prefers to act as an electron acceptor in the formation of electron donor−acceptor complexes, as demonstrated by the preferable interaction with DMAEMA relative to SAN or CNSt.

Overall, the results indicate that the formation of effective noncovalent interactions between polymer-bound functional groups and fullerenes can be controlled and optimized by minimizing steric restrictions of the polymer backbone to optimize the ability of the functional group to coordinate the interacting functional group with the fullerene near its optimized geometry. This geometry of the interaction plays a critical role in the extent of intermolecular interactions that can be realized between the polymer and C_{60}, which further impacts the dispersion and properties of polymer-fullerene nanocomposites.

AUTHOR INFORMATION

Corresponding Author
*E-mail: dad@utk.edu.

ACKNOWLEDGMENT

This research is supported by the Department of Energy, the Office of Basic Energy Sciences, and the Division of Materials Sciences and Engineering (S.T., M.D.D., and B.S.). Support from the National Science Foundation (D.L.) through grant DMR-0706323 is also acknowledged.

REFERENCES

(1) Goswami, M.; Sumpter, B. G. *J. Chem. Phys.* **2009**, *130*, 134910.
(2) Knauert, S. T.; Douglas, J. F.; Starr, F. W. *J. Polym. Sci.* **2007**, *45*, 1882–1897.
(3) Harris, P. J. *Carbon Nanotube Science: Synthesis, Properties and Application*; Cambridge University Press: New York, 2009.
(4) Ciprari, D.; Jacob, K.; Tannenbaum, R. *Macromolecules* **2006**, *39*, 6965–6573.
(5) Droste, D. H.; Dibenedetto, A. T. *J. Appl. Polym. Sci.* **1969**, *13*, 2149–2168.
(6) McIntosh, D.; Khabashesku, V. N.; Barrera, E. V. *J. Phys. Chem. C* **2007**, *111*, 1592–1600.
(7) Mitchell, C. A.; Bahr, J. L.; Arepalli, S.; Tour, J. M.; Krishnamoorti, R. *Macromolecules* **2002**, *35*, 8825–8830.
(8) Zhu, Y.; Wang, B.; Gong, W.; Kong, L.; Jia, Q. *Macromolecules* **2006**, *39*, 9441–9445.
(9) Tuteja, A.; Duxbury, P. M.; Mackay, M. E. *Phys. Rev. Lett.* **2008**, *100*, 077801.
(10) Laiho, A.; Ras, R. H. S.; Valkama, S.; Ruokolainen, J. *Macromolecules* **2006**, *39*, 7648–7653.
(11) Waller, J. H.; Bucknall, D. G.; Register, R. A.; Beckham, H. W.; Leisen, J.; Campbell, K. *Polymer* **2009**, *50*, 4199–4204.
(12) Linton, D.; Driva, P.; Sumpter, B.; Inanov, I.; Geohegan, D.; Feigerle, C.; Dadmun, M. D. *Soft Matter* **2010**, *6*, 2801.
(13) Rasheed, A.; Dadmun, M. D.; Ivanov, I.; Britt, P. F.; Geohegan, D. B. *Chem. Mater.* **2006**, *18*, 3513–3522.
(14) Rasheed, A.; Dadmun, M. D.; Britt, P. F. *Carbon* **2007**, *45*, 1 072–1080.
(15) Rasheed, A.; Dadmun, M. D.; Chae, H.-G.; Kumar, S. *Polymer* **2006**, *47*, 4734–4741.
(16) Rasheed, A.; Dadmun, M. D.; Britt, P. F. *J. Polym. Sci., Part B: Polym. Phys.* **2006**, *44*, 3053–3061.
(17) Kohn, W.; Becke, A. D.; Parr, R. G. *J. Phys. Chem.* **1996**, *100*, 12974–12980.
(18) Burns, L. A.; Vázquez-Mayagoitia, Á.; Sumpter, B. G.; Sherril, C. D. *J. Chem. Phys.* **2011**, *134*, 084107.
(19) Kobko, N.; Dannenberg, J. J. *J. Phys. Chem.* **2001**, *105*, 1944–1950.
(20) Mirau, P. A.; Lyons, M. *Macromolecules* **2010**, *43*, 625–629.
(21) Starr, F. W.; Schroder, T. B.; Glotzer, S. C. *Phys. Rev. E* **2001**, *64*, 021802.
(22) Lu, X.; Weiss, R. A. *Macromolecules* **1992**, *25*, 3242–3246.
(23) Wong, H. C.; Sanz, A.; Douglas, J. F.; Cabral, J. T. *J. Mol. Liq.* **2010**, *153*, 79–87.
(24) Tagmatarchis, N.; Prato, M. *Structure and Bonding*; Springer-Verlag: Berlin, Germany, 2004.
(25) Thompson, B. C.; Frechet, J. M. J. *Angew. Chem., Int. Ed.* **2008**, *47*, 58–77.
(26) Echegoyen, L.; Echegoyen, L. E. *Acc. Chem. Res.* **1998**, *31*, 593–601.
(27) Itoh, T.; Nitta, S.; Nonomura, S. *Appl. Surf. Sci.* **1997**, *113/114*, 282–285.